

Spin-reorientation transitions in cobalt nanowires: Role of the microstructure and finite-size effects

R. A. Guirado-López* and J. M. Montejano-Carrizalez†

Instituto de Física “Manuel Sandoval Vallarta,” Universidad Autónoma de San Luis Potosí, Alvaro Obregón 64, 78000 San Luis Potosí, Mexico

J. L. Morán-López‡

Institute for Computational Engineering and Science, University of Texas at Austin, Austin, Texas 78712-0027, USA

(Received 11 January 2008; revised manuscript received 12 March 2008; published 16 April 2008)

We present self-consistent electronic structure calculations in order to analyze the magnetocrystalline anisotropy energy as well as the local spin $S_{\delta}(i)$ and orbital $L_{\delta}(i)$ magnetic moments for finite-length Co nanowires. We consider monatomic chains, as well as single-crystal and polycrystalline nanowires, assuming two directions of magnetization δ oriented along ($\delta=x$) and perpendicular ($\delta=z$) to the wire axis. The single-crystal wires are cylindrical fragments of the fcc lattice grown along the (111) direction, while the polycrystalline structures are characterized by the presence of various fcc and hcp grains. We obtain that the Co chains are defined by a highly stable magnetization direction oriented along the chain axis. However, when three-dimensional wires are considered, we found a strong influence of the local atomic environment on the determination of the easy axis. In fact, we observe strong oscillations of the low energy orientation of the magnetization between the parallel and perpendicular directions as the length of the wire increases or when the geometrical details of the wire caps are modified. In contrast, in the polycrystalline structures, we found that the electronic perturbation introduced by the presence of internal interfaces is more localized in nature. Actually, no spin reorientation transitions are found for different microstructures; however, reduced energy differences (compared to uniform single-crystal wires with approximately the same length) between the parallel and perpendicular directions are obtained. Finally, the existence of internal interfaces can induce appreciable perturbations in the density of states around the Fermi energy and, as a consequence, they are expected to modify the number of conduction channels as well as the transport properties of the wires.

DOI: [10.1103/PhysRevB.77.134431](https://doi.org/10.1103/PhysRevB.77.134431)

PACS number(s): 75.75.+a

I. INTRODUCTION

Transition metal (TM) nanowires are one of the most studied magnetic nanostructures. In particular, a large amount of previous experimental reports have shown that single component as well as alloyed TM nanowire arrays synthesized by electrodeposition into porous membranes are relatively easy to fabricate (see, for example, Ref. 1 and references therein) and that they are characterized by having magnetic properties (e.g., hysteresis curves,²⁻⁴ Curie temperature,⁵ magnetization reversal mechanisms,^{2,6,7} etc.) that strongly depend on the wire length and diameter, inter-wire coupling, and microstructure, as well as chemical composition of the samples. Of course, revealing the precise correlation between the measured data and both the microscopic geometrical and chemical features is a fundamental issue (for both basic research and applied science) that needs to be addressed in order to achieve with success the possible applications of this kind of nanostructures in the magnetic recording technology and in the design of novel spintronic devices.

Interestingly, the structural characterization of these electrodeposited nanowires has revealed that their atomic configuration strongly depends on the synthesis protocol and, in this sense, the case of cobalt is the most illustrative. Actually, with the help of x-ray diffraction patterns as well as of both scanning and transmission electron microscopy images, it has been obtained, for example, that the as synthesized Co

nanowires (i) are in fact composed of several nanometer-sized grains with different geometrical phases, sizes, and relative orientations,^{2-4,8} (ii) are not perfectly aligned^{2,3,8} (i.e., it has been found that the angle between the wire axis and the normal to the film plane typically ranges between 0° and 30°), and (iii) their cross section is not uniform in the entire length of the wires, leading in some cases to constrictions and to significant deviations from the cylindrical shape.^{8,9} On the one hand, it is clear that the complex atomic organization of the wires within the pores is expected to have a strong influence on the measured macroscopic response of the samples and, on the other hand, their precise characterization is of course necessary also to adequately model their magnetic and electronic properties.

In this respect, a large amount of theoretical work has been reported in the past years in which mainly phenomenological approaches have been used to model very complex microscopic phenomena that occur in this kind of systems, for example, magnetization reversal mechanisms^{7,8,10} and the role played by the wire packing density and magnetostatic interactions,¹¹ as well as the domain wall motion within the wires.¹² In general, in these cases, the wires are mainly modeled as uniform assemblies of structureless cylinders or as chains of spheres or ellipsoids. However, despite the use of these simplified conditions, from these calculations, it has been possible to elucidate very interesting mechanisms that could be at the origin of experimentally measured magnetoresistance data and the behavior of magnetostatic interac-

tions in ordered nanowire arrays. Of course, it is clear that simplicity is a necessary requirement for massive simulations involving an assembly of wires with realistic size. However, it is reasonable to expect more accurate results (or the appearance of new phenomena) by taking into account the electronic structure of the species involved, as well as the precise geometrical details of the wires.

At this point, it is important to comment that more accurate semiempirical tight-binding studies and density functional theory calculations have been mainly restricted to the analysis of the structural and magnetic properties of one-dimensional atomic wires in the form of deposited^{13–18} or freestanding systems.^{19–21} In the former, monatomic chains with different lengths and chemical compositions have been deposited on both perfectly flat and stepped surfaces and interesting trends, concerning their structure and magnetic configuration, have been revealed. Furthermore, with the inclusion of the spin-orbit (SO) interaction in the model Hamiltonians, it has been possible to qualitatively estimate the role played by the magnetization direction on the transport properties of the wires²² as well as the values of the orbital moments in this kind of one-dimensional structures.^{15,16,21} In addition, the calculation of the magnetocrystalline anisotropy energy (MAE) has been particularly extensively addressed in the literature since it determines the low energy orientation of the magnetization within the structures via the SO interaction (which connects the spin moment to the atomic structure of a magnetic material).^{16,17,19–21} However, despite the large number of studies reported in the past years, to the best of our knowledge, little is known about the influence of more realistic geometrical imperfections such as polycrystallinity, finite-size effects, and the presence of internal defects on the magnetic properties of transition metal nanowires, particularly based on an electronic theory.

In this work, we thus present a systematic theoretical investigation dedicated to the analysis of the magnetic properties of finite-length Co nanowires with complex atomic configurations and with an aspect ratio that varies in the 8–63 range. We use a d -band tight-binding Hamiltonian treated in the unrestricted Hartree-Fock approximation, where the effects of the spin-orbit interaction (which allows us to calculate the orbital moment contributions to the total magnetization as well as the magnetic anisotropy energy) are non-perturbatively included. As was already commented above, cobalt was chosen because of its wide technological applications and rich nanometric behavior. Concerning the geometrical structure of our nanowires, we consider (i) monatomic chains and (ii) single^{9,23} and polycrystalline atomic configurations (guided by experimental results).^{2–4,8} The latter are characterized by the presence of various fcc and hcp grains with different sizes, which are stacked together to form metallic wires with contrasting surface terminations and with several internal interfaces. In all the cases, we consider two directions of the magnetization δ within the structures oriented along ($\delta=x$) and perpendicular ($\delta=z$) to the wire axis. We show that it is possible to obtain sizable variations in the magnitude and sign of the magnetic anisotropy energy (leading to strong oscillations of the easy axis between the parallel and perpendicular directions) when the length of the wire increases as well as when the geometrical

details of the wire caps or the internal structure is modified. As far as the electronic structure is concerned, we will also show that the density of states has a strong dependence on the magnetization direction and microstructure of the wires. We found sizable energy shifts and changes in the degeneracy of the eigenvalues in the entire electronic spectra: a result that is expected to strongly modify the number and orbital nature of the conduction channels in the structures.

The rest of the paper is organized as follows. In Sec. II, we briefly describe the theoretical model used for the calculations. In Sec. III, we present the discussion of our results and, finally, in Sec. IV, the summary and conclusions are given.

II. METHOD OF CALCULATION

Self-consistent semiempirical calculations have been performed for several Co nanowires by using the realistic d -band tight-binding Hamiltonian, which was proposed in Ref. 24, which nonperturbatively includes the intra-atomic Coulomb interactions in the unrestricted Hartree-Fock approximation and the effects of the spin-orbit coupling. The model has been described in detail elsewhere;^{25,26} thus, we only summarize its main points and discuss the choice of parameters.

Due to the inclusion of the SO interaction, the rotational invariance of the electronic Hamiltonian is no longer preserved and now depends on the orientation δ of the magnetization in the system. In the usual notation, the Hamiltonian is given by

$$H^\delta = \sum_{i\lambda,\sigma} \Delta \epsilon_{i\sigma}^\delta n_{i\lambda\sigma} + \sum_{i\lambda,j\mu,i \neq j,\sigma} t_{i\lambda,j\mu} c_{i\lambda\sigma}^\dagger c_{j\mu\sigma} + \sum_{i,\lambda\sigma,\mu\sigma'} \xi (\vec{L}_i \cdot \vec{S}_i)_{\lambda\sigma,\mu\sigma'} c_{i\lambda\sigma}^\dagger c_{i\mu\sigma'}, \quad (1)$$

where $c_{i\lambda\sigma}^\dagger$ ($c_{i\lambda\sigma}$) refers to the creation (annihilation) operator of an electron with spin σ in the d orbital λ at atomic site i and $n_{i\lambda\sigma} = c_{i\lambda\sigma}^\dagger c_{i\lambda\sigma}$ defines the electron number operator. The first term of Eq. (1), $\Delta \epsilon_{i\sigma}^\delta$, corresponds to the site- and spin-dependent energy shift of the d level, $\epsilon_{i\sigma} = \epsilon_d^0 + \Delta \epsilon_{i\sigma}^\delta$ (where ϵ_d^0 stands for the d orbital energy in the paramagnetic bulk) and is determined by the global charge and the spin as follows:

$$\Delta \epsilon_{i\sigma}^\delta = U(i) \Delta n^\delta(i) - \sigma J(i) S_\delta(i), \quad (2)$$

with $\Delta n^\delta(i) = n^\delta(i) - n_d(\text{bulk})$. The average intra-atomic direct Coulomb repulsion integral is denoted by U and the average exchange integral is denoted by J . The spin-quantization axis is taken to be parallel to the magnetization direction, which is assumed to be uniform within the wires. The second term of Eq. (1), $t_{i\lambda,j\mu}$, denotes the corresponding hopping integrals between sites i and j and orbitals λ and μ , and finally, the third term corresponds to the SO interaction treated in the usual intra-atomic single-site approximation.^{27,28} Here, ξ stands for the SO-coupling constant and $(\vec{L}_i \cdot \vec{S}_i)_{\lambda\sigma,\mu\sigma'}$ refers to the intra-atomic matrix elements of $\vec{L} \cdot \vec{S}$, which couple the up and down spin manifolds and which depend on the relative orientation between the magnetization direction and the

wire lattice. The number of d electrons at site i ,

$$n^\delta(i) = \sum_\lambda (\langle n_{i\lambda\uparrow}^\delta \rangle + \langle n_{i\lambda\downarrow}^\delta \rangle), \quad (3)$$

and the local spin $\vec{S}(i)=[S_x(i), S_y(i), S_z(i)]$ at each cluster site i and for a given direction of magnetization δ ,

$$S_\delta(i) = \frac{1}{2} \sum_\lambda (\langle n_{i\lambda\uparrow}^\delta \rangle - \langle n_{i\lambda\downarrow}^\delta \rangle), \quad (4)$$

are self-consistently calculated by integrating the local density of states (LDOS) $\rho_{i\lambda\sigma}^\delta(\varepsilon) = -(1/\pi)\text{Im}\{G_{i\lambda\sigma, i\lambda\sigma}^\delta(\varepsilon)\}$, where $G^\delta(\varepsilon)=[\varepsilon - H^\delta]^{-1}$ is the Green function operator up to the Fermi level ε_F , which is determined by the number of d electrons per atom in the wires.

The local orbital moments $L_\delta(i)$ at each wire site are calculated from

$$L_\delta(i) = \sum_\sigma \sum_{m=-2}^{m=2} \int_{-\infty}^{\varepsilon_F} m \rho_{im\sigma}^\delta(\varepsilon) d\varepsilon, \quad (5)$$

where the real d orbitals have been transformed to the complex spherical harmonics basis and m refers to the magnetic quantum number. Here, the quantization axis of the orbital momentum is the same as the spin-quantization axis.

The electronic energy $E_\delta = \sum_i E_\delta(i)$ can be written as the sum of local contributions:

$$E_\delta(i) = \sum_{\lambda\sigma} \left[\int_{-\infty}^{\varepsilon_F} \varepsilon \rho_{i\lambda\sigma}^\delta(\varepsilon) d\varepsilon - E_{i\lambda\sigma}^{\text{dc}} \right], \quad (6)$$

corresponding to the different atoms i within the wires, where $E_{i\lambda\sigma}^{\text{dc}}$ stands for the double-counting correction. The MAE is defined as the change ΔE in the electronic energy E_δ associated with a change in the orientation of the magnetization. In this work, for each cobalt nanowire, we consider two directions of the magnetization δ , which are oriented along ($\delta=x$) and perpendicular ($\delta=z$) to the wire axis. However, it is important to comment that the magnetization direction can be chosen without restrictions. Actually, by taking advantage of our local approach, it is possible to express the total energy difference ΔE_{xz} between two arbitrary orientations $\delta = x, z$ as a sum of atom resolved contributions:

$$\Delta E_{xz} = \sum_i \Delta E_{xz}(i) = \sum_i [E_x(i) - E_z(i)], \quad (7)$$

where $E_\delta(i)$ is given by Eq. (6). Thus, the global magnetoanisotropic properties can be related to the various local atomic environments within the wires. The LDOSs $\rho_{i\lambda\sigma}^\delta(\varepsilon)$ are determined by performing independent self-consistent calculations for each orientation of the magnetization δ by using the Haydock-Heine-Kelly recursion method²⁹ and, in this way, we derive the MAE in a nonperturbative fashion as a difference between electronic energies.

III. RESULTS AND DISCUSSION

In this section, we present the local atomic environment dependence of both the spin and orbital magnetic moments,

as well as of the MAE, together with the resulting low energy orientations of the magnetization within our considered cobalt nanowires. The parameters used for the calculations are obtained from bulk properties (d -band width, equilibrium distance, and bulk magnetic moment) as follows. The two-center d electron hopping integrals ($dd\sigma$, $dd\pi$, $dd\delta$) are defined by the canonical expressions given by Heine,³⁰ varying as the inverse fifth power of the interatomic distance r [$dd\sigma = -6(W_b/2.5)(r_{WS}/r)^5$, $dd\pi = 4(W_b/2.5)(r_{WS}/r)^5$, and $dd\delta = -1(W_b/2.5)(r_{WS}/r)^5$] in terms of the corresponding bulk d -band width of Co,³¹ $W_b(\text{Co}) = 5.5$ eV, and the Wigner-Seitz radius r_{WS} . Charge transfer effects are treated in the limit of a large direct Coulomb repulsion $U(i)$ [i.e., $U(i) \rightarrow +\infty$ and $\Delta n(i) \rightarrow 0$ with $U(i)\Delta n(i)$ finite], which amounts to imposing a local charge neutrality at each site i . The values for the d -band filling $n_d(\text{Co}) = 8.3$ and intra-atomic exchange integral $J_{\text{Co}} = 0.76$ eV (fitted to reproduce the proper magnetic moment and exchange splitting in the bulk), as well as the SO-coupling constant $\xi_{\text{Co}} = 88$ meV (obtained from Ref. 28), have already been used in previous works.^{25,32,33}

A. Magnetic properties of Co monatomic chains

We first study the magnetic properties of finite-length monatomic Co chains. We consider two directions of the magnetization, which are oriented along ($\delta=x$) and perpendicular ($\delta=z$) to the wire axis, and we use a fixed nearest neighbor interatomic distance between Co atoms, being equal to $R_o = 2.5$ Å.

In all our considered wires, we have found that the modulus of the spin moment $|\vec{S}|$ very weakly depends on the direction of magnetization δ , therefore, for each one of our considered atomic chains, we will only refer to the results for $2S_z$. Actually, in addition to this weak dependence on δ , in all our one-dimensional structures, we have also found almost saturated local spin moments $2S_z(i) \sim 1.7\mu_B$ in all the sites i and, as a consequence, $2S_z$ is not so sensitive either to the local atomic environment or to the length l of the chains. This behavior is characteristic of magnetic nanostructures defined by a large exchange regime and has been also found in various types of magnetic systems such as in TM clusters with different sizes and symmetries,^{32,34} as well as in magnetic thin films with different packings.³⁵

However, in contrast to the independence of the spin moments of δ , i , and l , we see from Fig. 1 that the local orbital magnetic moments $L_\delta(i)$ for Co₁₉ [Fig. 1(a)], Co₄₉ [Fig. 1(b)], and Co₈₉ [Fig. 1(c)] monatomic wires (shown as representative examples) are more sensitive to variations in the direction of the magnetization and in the local atomic environment. From the figure, we first note that very enhanced values for $L_\delta(i)$, with respect to the hcp Co bulk ($L_z = 0.14\mu_B$), are found in all our chains, the largest enhancement being obtained in general at the sites located at the end of the wires where $L_\delta(i) \sim 1\mu_B$. However, we notice that a sizable part of this increase in the local orbital moments is considerably lost when we move to the inner regions of the atomic chains, where $L_\delta(i)$ decays very fast (with some oscillations) with increasing the distance from the extremes of the chains. Interestingly, in all our considered wires, we ob-

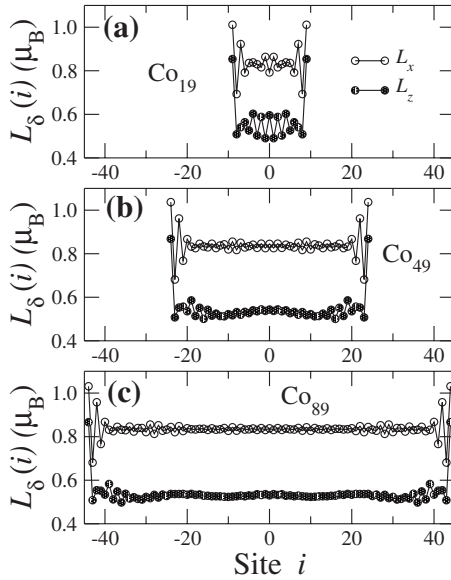


FIG. 1. Calculated local orbital moments $L_{\delta}(i)$ (μ_B) for (a) Co_{19} , (b) Co_{49} , and (c) Co_{89} monatomic wires.

serve almost the same value for $L_{\delta}(i)$ at the center of the structures, being of the order of $0.5\mu_B$ for $\delta=z$ and of $0.8\mu_B$ for $\delta=x$. These values could be representative of the infinite chain limit and, actually, they are very close to the ones calculated by Komelj *et al.*¹⁵ for monatomic Co wires by means of *ab initio* techniques, which is a fact that gives us confidence in our results.

It is important to also comment about the difference $L_z(i) - L_x(i) = \Delta L_{zx}$ of the calculated local orbital moments in each site i between the two different orientations of the magnetization. From Fig. 1, we also note that sizable values for ΔL_{zx} vs i are found, being as large as $0.4\mu_B$ (at the sites located at the wire caps), which are orders of magnitude larger than the values for ΔL_{zx} previously found at magnetic transition metal surfaces²⁵ and nanoparticles.³³ It is important to be precise that the magnitude and sign of ΔL_{zx} are particularly relevant due to the well known (second order perturbation theory) expression that relates both the anisotropy in the orbital moments to the anisotropy in the electronic energies through the proportionality equation $L_z - L_x \propto E_x - E_z$.²⁸ This relation implies that the easy axis in the systems can be also inferred by determining (e.g., by means of x-ray magnetic circular dichroism experiments³⁶) the direction of magnetization δ characterized by the largest value of the orbital moment. Following these arguments, we can thus clearly predict from Fig. 1 that the direction $\delta=x$ will define the low energy orientation of magnetization in all our considered monatomic wires.

In fact, this is what we observe in Fig. 2, where we plot the average magnetic anisotropy energy, $\langle \Delta E_{xz} \rangle$, as a function of the length l of our considered chains calculated by Eq. (7). From the figure, we clearly see that, in all cases, sizable negative values for $\langle \Delta E_{xz} \rangle$ are found, which is a fact that implies that the low energy direction of the magnetization is oriented along the wire axis ($\delta=x$), which is in agreement with the orbital magnetization data shown in Fig. 1. This result is also consistent with previous calculations reported

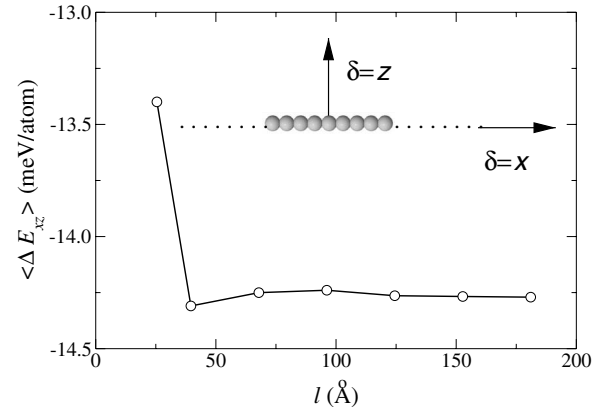


FIG. 2. Average magnetic anisotropy energy, $\langle \Delta E_{xz} \rangle$ (meV/atom), calculated for our considered monatomic wires as a function of their length l (\AA). In the inset, the two magnetization directions are shown.

in Ref. 17 for both finite and infinite monatomic Co chains where a highly stable magnetization direction along the wire axis was found. In addition, in that work, it was clearly shown that the interaction of Co chains with a Pd surface could strongly perturb their magnetic properties, being at the origin of spin reorientation transitions in the systems. However, we believe that the here-reported trends are expected to hold in the case of weakly interacting substrates (i.e., negligible charge transfer), such as insulating films or semiconducting surfaces, where only sizable perturbations in the nearest neighbor interatomic distance between the Co atoms in the deposited chains are expected to occur.

In fact, in order to analyze these structural effects, we have performed additional calculations to study the magnetic properties of more realistic strained Co monatomic wires. We have chosen the Co_{19} , Co_{49} , and Co_{89} chains (already analyzed in Fig. 1) as representative examples. In all cases, we have found that uniform contractions or expansions in the Co-Co bond length, at least as large as 5%, are not enough to change the low energy direction of the magnetization calculated in Fig. 2, defining, as a consequence, a highly stable spin orientation in the one-dimensional systems.

B. Magnetic properties of single-crystal fcc Co nanowires

In this section, we now analyze the magnetic properties of finite-length single-crystal fcc nanowires, as the ones shown in Fig. 3. These cylindrical structures are compact portions of the fcc lattice grown along the (111) direction. In the figure, we show as representative examples the wire structures for Co_{111} [Fig. 3(a)], Co_{117} [Fig. 3(b)], Co_{123} [Fig. 3(c)], and Co_{125} [Fig. 3(d)]. They are all formed by a central atomic chain placed along the x axis surrounded by two successive coaxial shells (made of triangular and hexagonal units), resulting in ultrathin wire structures with an average diameter equal to 3.9\AA . Notice from the figure that nanowires with different lengths can also differ in the atomic structure of their wire caps, which is a fact that, as will be seen in the following, will play a fundamental role in determining the average magnetoanisotropic behavior in the systems.

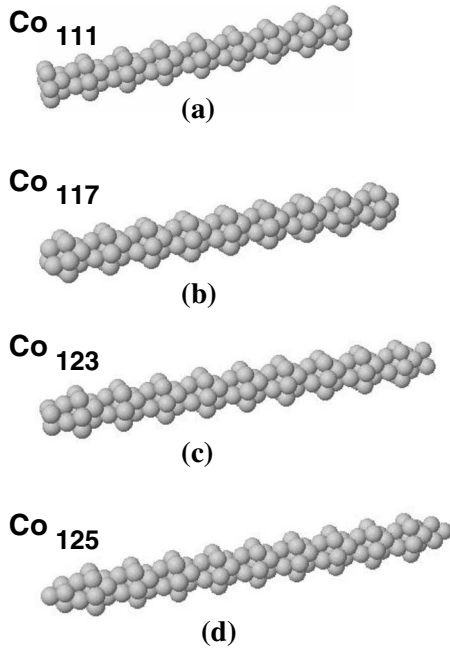


FIG. 3. Illustration of our considered single-crystal fcc nanowires grown along the (111) direction for (a) Co_{111} , (b) Co_{117} , (c) Co_{123} , and (d) Co_{125} .

In Fig. 4, we show our results for the calculated average magnetic anisotropy energy, $\langle \Delta E_{xz} \rangle$, as a function of the length l of our considered single-crystal Co nanowires (see Fig. 3 for representative examples). In contrast to the results plotted in Fig. 2, we now observe in Fig. 4 that the $\langle \Delta E_{xz} \rangle$ vs l curve presents strong oscillations in the MAE values, which dramatically changes not only in magnitude but also in sign, leading to the existence of various spin reorientation transitions in the systems as l increases. Actually, even if our nanowires with $l > 45 \text{ \AA}$ are characterized by having the same low energy direction of the magnetization [$\langle \Delta E_{xz}(l) \rangle > 0$], being oriented perpendicular to the wire axis, we can see that sizable variations in the magnitude of $\langle \Delta E_{xz} \rangle$ are still observed. In particular, it is important to remark on the pres-

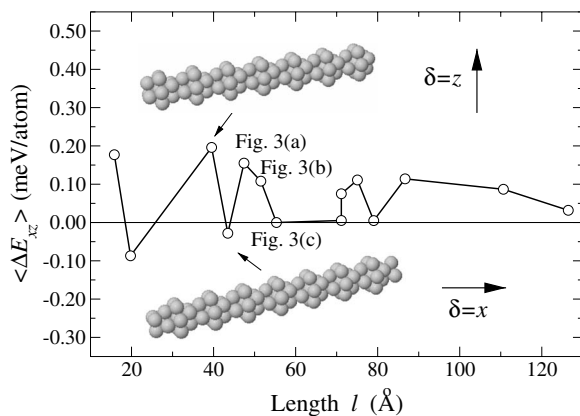


FIG. 4. Average magnetic anisotropy energy, $\langle \Delta E_{xz} \rangle$ (meV/atom), calculated for our considered single-crystal fcc nanowires as a function of their length l (Å). In the insets, we show the structures of the Co_{91} and Co_{97} wires.

ence of Co nanowires with $\langle \Delta E_{xz} \rangle \approx 0$ since these values, on the one hand, imply a low stability of the magnetization direction and the existence of reduced blocking temperatures within the wires and, on the other hand, also define a scenario in which minor structural transformations, or electronic perturbations (charge transfer originated from the adsorption of contaminants or ligands), might influence the orientation of the easy axis in the structures.

At this point, it is important to comment that besides the spin reorientation transitions observed in Fig. 4 as l increases, we have found that structures with approximately the same length but with a different geometrical arrangement at the wire caps also exhibit a complex magnetic behavior. This is clearly seen, for example, in the cases of the Co_{91} ($l=39.5 \text{ \AA}$) and Co_{97} ($l=43.5 \text{ \AA}$) wires, which are shown as insets in Fig. 4. Here, the latter is constructed from the former by simply adding an additional triangular unit to both ends of the Co_{91} wire, defining a new Co structure with almost the same aspect ratio, being approximately equal to ~ 20 . However, from the figure, we see that this minor structural modification is enough to modify the low energy orientation of the magnetization in the system from being perpendicular [$\langle \Delta E_{xz} \rangle > 0$] to being parallel [$\langle \Delta E_{xz} \rangle < 0$] to the wire axis. Interestingly, even if localized in nature, the previous geometrical modification of the wire caps causes, as we will see in the following, an extended electronic perturbation within the wire that considerably changes the local contributions $\Delta E_{xz}(i)$ [see Eq. (6)] in the system, modifying, as a consequence, the global average magnetoanisotropic behavior. Actually, if we now add to the Co_{97} nanowire an additional hexagonal cluster to each one of its ends, we obtain a Co_{111} structure with a length of 47.5 \AA [see Fig. 3(a)]. In this case, a new spin reorientation transition is found, and the low energy direction of the magnetization comes back (as in the Co_{91} case) to being perpendicular to the wire axis. Finally, it is important to remark that for the larger wires, the sign of $\langle \Delta E_{xz} \rangle$ is stabilized leading in all cases to a direction of magnetization perpendicular to the wire axis, which is in contrast to the one-dimensional case (see Fig. 2).

It is interesting to correlate the average magnetic behavior of our Co nanowires shown in Fig. 4 with the different local anisotropies $\Delta E_{xz}(i)$ obtained within our considered structures. In Fig. 5, we first show for some representative cases the average contributions $\langle \Delta E_{xz}(j) \rangle$ for the different axial shells j surrounding the principal symmetry axis of our wires. In the figure, $j=1$ defines the Co atoms located on the x axis forming a monatomic (expanded) chain (see the inset of the figure), $j=2$ specifies the atoms forming the triangular clusters which are found all along the cylindrical structures, being placed at a distance of 1.43 \AA from the principal symmetry axis of the wires, and, finally, $j=3$ defines the Co atoms located in the hexagonal units at a distance of 2.48 \AA from the center of the structures. In Fig. 5, we show our results for Co_{45} , Co_{91} , Co_{97} , Co_{111} , and Co_{123} nanowires for which an interesting average magnetoanisotropic behavior has been obtained (see Fig. 4). From the figure, we first note that the local contributions $\langle \Delta E_{xz}(j) \rangle$ strongly change as a function of j , as well as when the length of the nanowires is modified. It is important to remark that, in general, the values of $\langle \Delta E_{xz}(j) \rangle$ for the surface positions $j=2$ and $j=3$ have in

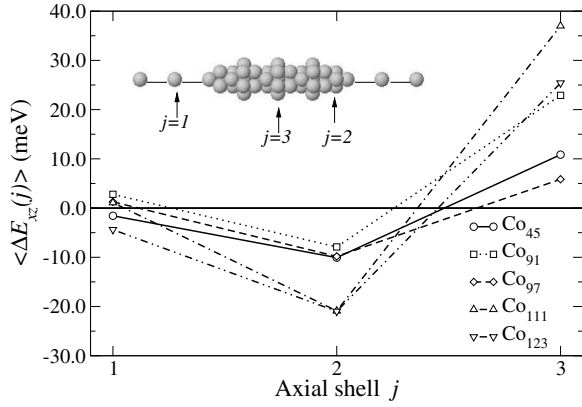


FIG. 5. Calculated average magnetic anisotropy energy, $\langle \Delta E_{xz}(j) \rangle$ (meV), as a function of the axial atomic shell of neighbors j for some selected Co nanowires. In the inset, we show a representative volume of our considered structures in which some of the surface sites have been removed in order to evidence the location of the atoms located on the principal axis of the wires ($j=1$), as well as the triangular ($j=2$) and hexagonal ($j=3$) units.

most of the cases the same magnitude but different sign, resulting in nonadditive contributions that yield very small values for the sum $\langle \Delta E_{xz}(2) \rangle + \langle \Delta E_{xz}(3) \rangle$. In contrast, the energy variations of $\langle \Delta E_{xz}(1) \rangle$, even if they cover a more reduced energy range, can change sign and, actually, as we will see in the following, they play an important role in defining the low energy orientation of the magnetization in the systems.

The previous trends are clearly seen in the case of the Co₄₅ nanowire (see the continuous line) where the local contributions for $j=2$ and $j=3$ tend to cancel each other, yielding a very small but positive value and, as a consequence, the negative local contribution obtained for $j=1$ is thus at the origin of the low energy orientation of the magnetization along the x axis (Fig. 4). In contrast, for the Co₉₁ structure, both $j=1$ and $j=3$ local contributions are now positive and thus dominate the average magnetic behavior, being actually at the origin of the switch of the magnetization from along to perpendicular to the wire axis.

The analysis of the axial distribution of the local magnetic anisotropy energies discussed in the previous paragraph has already revealed an interesting behavior for $\langle \Delta E_{xz}(j) \rangle$ as a function of the local atomic environment. However, the slow convergence of $\langle \Delta E_{xz} \rangle$ as a function of l , as well as the high sensitivity of the low energy magnetization direction to the geometrical structure of the wire caps (shown in Fig. 4), also points to the existence of strong finite-size effects in this kind of systems. Consequently, and with the purpose of more clearly understanding the length dependence of the MAE shown in Fig. 4, we divide our considered single-crystal fcc Co nanowires into three fragments F_i : (i) one located in the central region of the wires, F_c , with a length of 11.8 Å and (ii) two equal wire volumes (with varying length) located to the right, F_r , and to the left, F_l , of the central region defining the end portions of our structures.

In Fig. 6, we plot the individual average MAE contributions of these representative volumes as a function of l . From this figure, we can see that, in contrast to the total MAE vs l

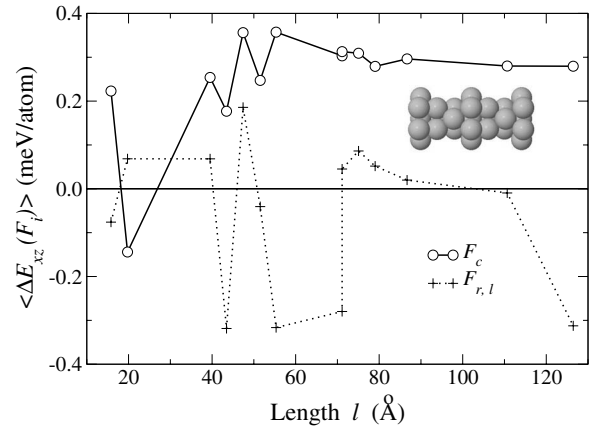


FIG. 6. Calculated average magnetic anisotropy energy, $\langle \Delta E_{xz}(F_i) \rangle$ (meV/atom), for selected fragments (see text) in our considered single-crystal fcc nanowires as a function of their length l (Å). In the inset, we show the structure of the central volume (with 33 atoms and length $l=16.7$ Å) considered in all cases.

shown in Fig. 4, the average MAE of the central volume $\langle \Delta E_{xz}(F_c) \rangle$ (shown as inset) is always positive (with the exception of the Co₄₅ case) and slowly varies as a function of l . Still, we observe that for nanowires with $l < 80$ Å, the average contribution of the MAE in the central region is clearly affected by the size and structure of the wire caps. However, from the figure, we note that for nanowires with $l > 80$ Å, the MAE contribution of this portion becomes almost constant. In fact, the magnetic anisotropy energy is always positive and appears to saturate to 0.3 meV/atom, which thus gives an idea of the values one would obtain for an ideal infinite fcc Co nanowire of this diameter. Actually, the average orbital moment of this region $\langle L_\delta(F_c) \rangle$ is equal to $0.26\mu_B$, still being notably enhanced with respect to the bulk value.

From Fig. 6, we note in contrast that a more complex magnetic behavior is obtained for the Co segments located at the wire caps. In fact, when compared with the results shown in Fig. 4, we notice that the average MAEs as a function of l in these fragments $\langle \Delta E_{xz}(F_{r,l}) \rangle$ are the ones that dominate the global average magnetic behavior, strongly contributing to the observed spin reorientation transitions and to the reduced values of $\langle \Delta E_{xz} \rangle$ with increasing the length of the wires. These results clearly demonstrate that nanowires of these lengths can yield different contributions for the $\langle \Delta E_{xz} \rangle$ depending on the particular way the structures are terminated.

C. Magnetic properties of polycrystalline Co nanowires

In this section, we now present the magnetic properties of finite-length polycrystalline Co nanowires. Some of our considered polycrystalline structures are shown in Fig. 7 and are characterized by the presence of various fcc and hcp grains with different sizes, which are grown along the (111) and x directions, respectively, and are stacked together to form metallic wires with contrasting surface terminations and with several internal interfaces. In Fig. 7(a), we first show the structure of a single fcc wire made of 195 atoms. In Fig. 7(b), we show the case of a Co nanowire with 183 atoms and made of three fcc fragments, each one of them having a

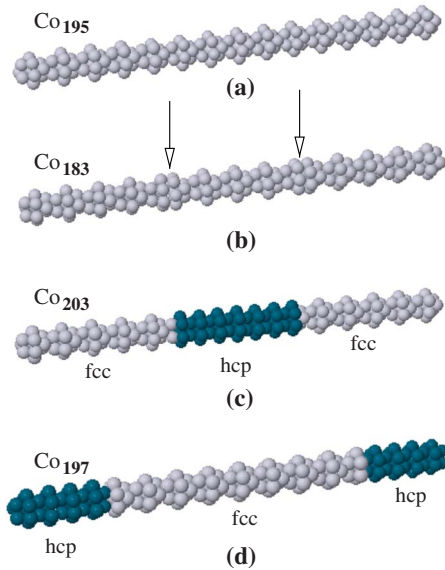


FIG. 7. (Color online) Illustration of our considered polycrystalline Co nanowires. (a) A single fcc Co_{195} structure grown along the (111) direction. (b) Co_{183} wire composed of three fcc segments rotated with respect to each other by 30° , being attached through hexagonal units (see the arrows). (c) A polycrystalline Co_{203} nanowire made by a central hcp fragment (blue spheres) to which we attach in both sides a fcc portion (gray spheres). (d) A polycrystalline Co_{197} structure made by a central fcc fragment (gray spheres) to which we attach in both sides a hcp portion (blue spheres).

length $l \sim 25 \text{ \AA}$. These fragments are attached together through the hexagonal units (as marked by arrows in the figure) and are rotated with respect to each other by 30° . Notice that, compared with the single-crystal wire shown in Fig. 7(a), the different relative orientations between the segments leads to the formation of a Co nanowire with a more corrugated surface.

In Fig. 7(c), we present a Co cylindrical structure in which the central region of the nanowire is made of a cylindrical hcp fragment with 67 atoms and length $l=25 \text{ \AA}$ (see blue spheres) to which we add, in both sides, a fcc grain with 68 atoms and a length of 31.4 \AA . As seen from the figure, the two types of structures are attached through a junction involving a triangular cluster and a hexagonal unit. In Fig. 7(d), a similar type of construction is presented but now the fcc fragment is the one located in the center of the wire and the hcp fragments are found to be attached to the left and to the right of the hcp cylindrical segment. Notice that, compared to the single-crystal structure shown in Fig. 7(a), all our considered polycrystalline wires are approximately of the same length (varying by at most $\pm 7 \text{ \AA}$) but strongly differ in their microstructure. Finally, it is important to comment that even if the previous types of constructions roughly model the structural features reported for this kind of systems,^{2-4,8} we believe that our here-proposed atomic configurations contain the fundamental ingredients necessary to analyze the changes in the local magnetic moments and MAE values due to the existence of a nonperfect growth.

In Fig. 8, we show our results for the calculated average magnetic anisotropy energy, $\langle \Delta E_{xz} \rangle$, for the polycrystalline

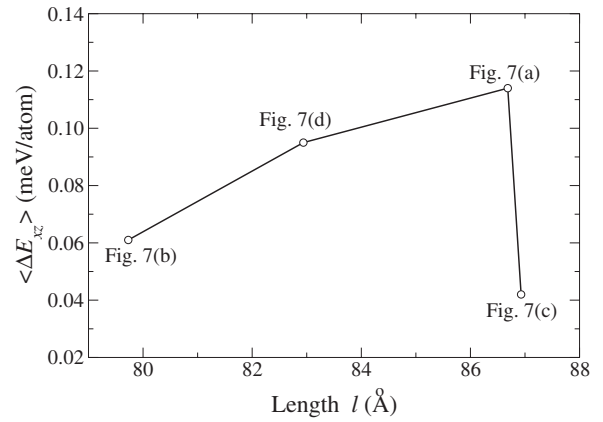


FIG. 8. Average magnetic anisotropy energy, $\langle \Delta E_{xz} \rangle$ (meV/atom), calculated for the wire structures shown in Fig. 7.

structures shown in Figs. 7(b)–7(d). We also include in the figure, for the sake of comparison, our calculated value for $\langle \Delta E_{xz} \rangle$ for the single-crystal atomic configuration shown in Fig. 7(a). From the figure, we see as a general trend that, when considering a grainlike structure for Co nanowires, the energy difference $\langle \Delta E_{xz} \rangle$ between the parallel and perpendicular directions of magnetization (compared to the single-crystal wire) is always reduced. This is particularly the case when both fcc and hcp phases coexist within the structures, as seen from our data shown in Fig. 8 for the Co_{203} nanowire with a length of 87 \AA . Still, the calculated values for $\langle \Delta E_{xz} \rangle$ are larger than the ones found for bulk hcp Co ($\sim 10^{-5} \text{ eV}$). Interestingly, and in contrast to the results shown in Fig. 4, we notice that introducing this kind of structural imperfections does not lead to spin reorientation transitions in the systems. However, our results shown in Fig. 8 could imply that, in real samples, reducing the degree of polycrystallinity might lead to the formation of magnetic nanowires with a more stable low energy magnetization direction.

Actually, as shown in the previous section, it is possible to trace the sizable reduction in the MAE values for the polycrystalline atomic configurations shown in Fig. 8 to the already observed sensitivity of ΔE_{xz} to the local atomic environment. In particular, it is interesting to analyze the average MAE contributions of each one of the grains and how they combine to define the average magnetoanisotropic behavior of the wires. In this respect, we show in Fig. 9 the average MAE contributions $\langle \Delta E_{xz}(V_i) \rangle$ for well defined volumes, V_i ($i=\text{fcc}$ and hcp), for the Co nanowires as the ones shown in Fig. 7. In the figure, we indicate the corresponding value of $\langle \Delta E_{xz}(V_i) \rangle$ for each one of the selected volumes V_i as well as the average MAE in the structures. From Fig. 9(b), we first see that by simply introducing a small degree of orientational disorder in a single-crystal structure, a sizable reduction in the total MAE is obtained [compare with Fig. 9(a)]. Note that, in contrast to the results shown in Fig. 9(a), the end portions of the wires now contribute with small positive values, which are of the order of $\sim 0.034 \text{ meV/atom}$, thus dominating the global magnetoanisotropic behavior, and begin at the origin of the notable reduction in the total MAE.

From Fig. 9(c), a more interesting behavior is observed since, besides the small and positive values obtained for

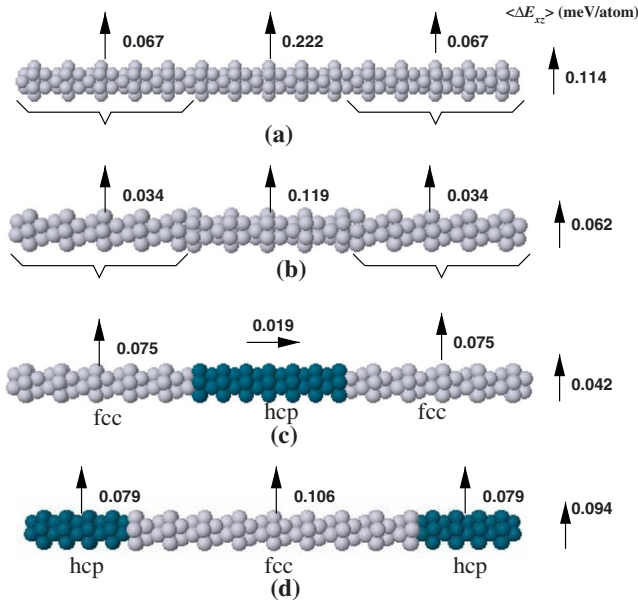


FIG. 9. (Color online) Calculated average magnetic anisotropy energy, $\langle \Delta E_{xz}(V_i) \rangle$ (meV/atom), for selected fragments (as indicated in the figure) for the Co nanowires shown in Fig. 7. The low energy orientation of the magnetization of each volume V_i is indicated by an arrow. To the right of each figure, we also show the calculated value for $\langle \Delta E_{xz} \rangle$ (meV/atom).

$\langle \Delta E_{xz}(V_{fcc}) \rangle$ in the fcc fragments located at the end of the wires, the average local contribution of the hcp grain $\langle \Delta E_{xz}(V_{hcp}) \rangle$ is found to be negative, implying that the low energy direction of magnetization in this well defined volume is oriented along the x axis. Of course, these local values result in nonadditive contributions that are at the origin of a more reduced MAE value, as indicated in the figure. Finally, and in contrast to the results shown in Fig. 9(c), from Fig. 9(d), we see that hcp fragments located at the wire caps have an average magnetization oriented perpendicular to the wire axis [$\langle \Delta E_{xz}(V_{hcp}) \rangle > 0$], similar to the central fcc volume, which is a contribution that reinforces the spin direction perpendicular to the wire as the easy axis of the structure. Interestingly, this kind of grainlike structure has been observed in real samples of Co nanowire arrays fabricated by electrodeposition¹ or naturally appear if the wires are formed through the aggregation of nanoparticles technique.³⁷ We can thus conclude by saying that a detailed characterization of the wire structure should be very important for a precise characterization of the material properties, as well as for more realistic comparisons between theory and experiments.

The role of the presence of grain boundaries on the local distribution of the orbital moments and magnetic anisotropy energies can be also analyzed by plotting the average values of $\langle \Delta E_{xz} \rangle$ and $\langle L_\delta \rangle$ found for both the hexagonal and triangular units, as well as for the single Co atoms located all along the length of the wire defining different shells m ($m=0$ being the center of the wire). These data are plotted in Figs. 10–12 for single-crystal Co₁₉₅ and polycrystalline Co₁₈₃ and Co₂₀₃ structures, respectively, which are shown in Figs. 7(a)–7(c).

From Figs. 10(a) and 10(b), we see that, for the single-crystal wire, a highly regular distribution for both $\langle \Delta E_{xz}(m) \rangle$

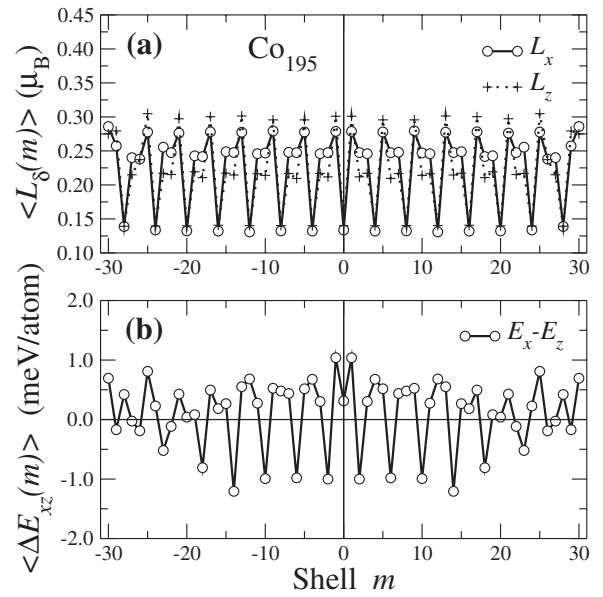


FIG. 10. (a) Average local orbital moments, $\langle L_\delta(m) \rangle$ (μ_B), for the single-crystal Co₁₉₅ wire shown in Fig. 7(a) as a function of the shell m (see text). (b) Same as in (a) but for the average local magnetic anisotropy energy, $\langle \Delta E_{xz}(m) \rangle$ (meV/atom).

and $\langle L_\delta(m) \rangle$ as a function of m is obtained within the structure. However, from Figs. 11 and 12, it is interesting to remark that the previously well defined sequence of values obtained for $\langle \Delta E_{xz}(m) \rangle$ and $\langle L_\delta(m) \rangle$ are notably perturbed, particularly in Fig. 12, wherein different geometrical phases coexist within the wire. Notice that the local anisotropies are more strongly affected by the presence of these grain boundaries, leading to a highly nonuniform $\langle \Delta E_{xz} \rangle$ vs m curve but with a more equilibrated distribution of positive and negative contributions. The previous local distribution leads to strong cancellation effects, thus being responsible for the sizable quenching of the average MAE found in Fig. 8.

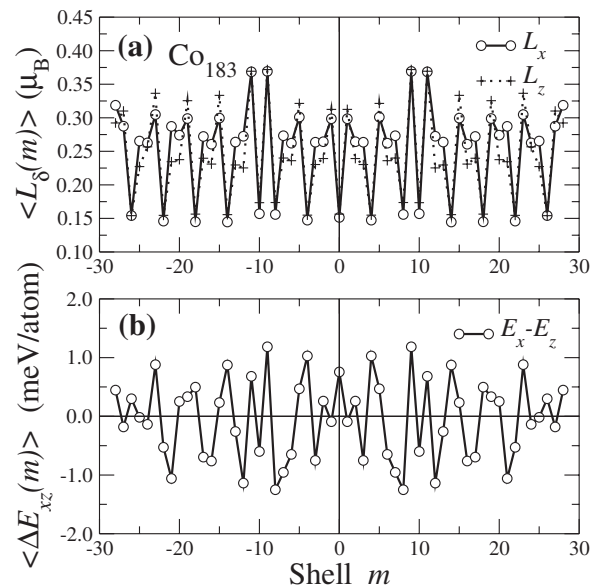


FIG. 11. Same as in Fig. 10 but for the Co₁₈₃ nanowire shown in Fig. 7(b).

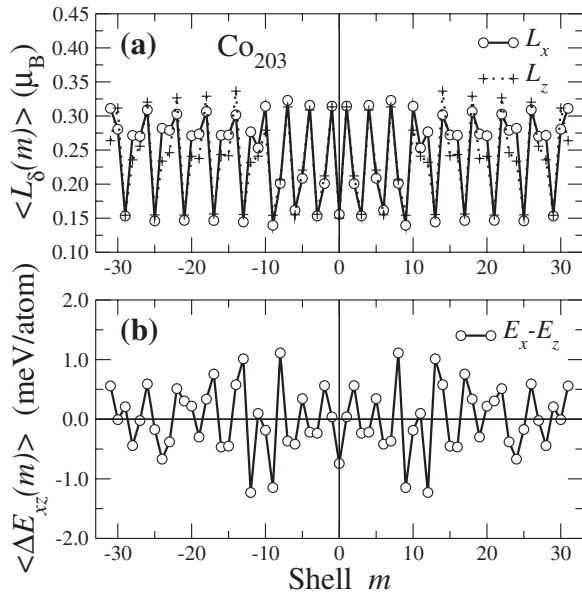


FIG. 12. Same as in Fig. 10 but for the Co_{203} nanowire shown in Fig. 7(c).

We believe that the previous results obtained for both single-crystal and polycrystalline Co nanowires are particularly relevant when they are set in the form of an array since the different values found for the average MAE, for the different types of microstructure, will compete or add with the other magnetic anisotropy energy contributions such as the shape anisotropy or dipolar interactions, thus playing a fundamental role in defining the average magnetic properties of the samples.

D. Calculation of the density of states

As is well known, previous theoretical works performed on transition metal clusters,¹⁹ monatomic wires,^{19,20,22} and thin films³⁸ have shown that changing the spin orientation within the structures leads to significant perturbations in their electronic spectra, consisting in sizable energy shifts as well as in changes in the degeneracy of the eigenvalues (induced by the SO coupling) occurring all along the energy level distribution. In fact, the previous electronic perturbations have been found to be of fundamental importance (when they are present around the Fermi energy) for determining the magnitude of the anisotropy barriers between the two directions of magnetization as well as for explaining the spin reorientation transitions observed in this kind of magnetic nanostructures.

In order to show these effects in our considered Co nanowires, we plot in Figs. 13 and 14 the average density of states (ADOS) of single-crystal Co_{195} [Fig. 7(a)] and polycrystalline Co_{183} [Fig. 7(b)] structures, respectively, for the two considered directions of magnetization δ . From the figures we see in both cases an appreciable dependence of the ADOS on the orientation of the magnetization. As expected, we found the existence of notable energy shifts and SO-coupling-induced removal of degeneracies all along the energy range. This is particularly the case in the polycrystalline

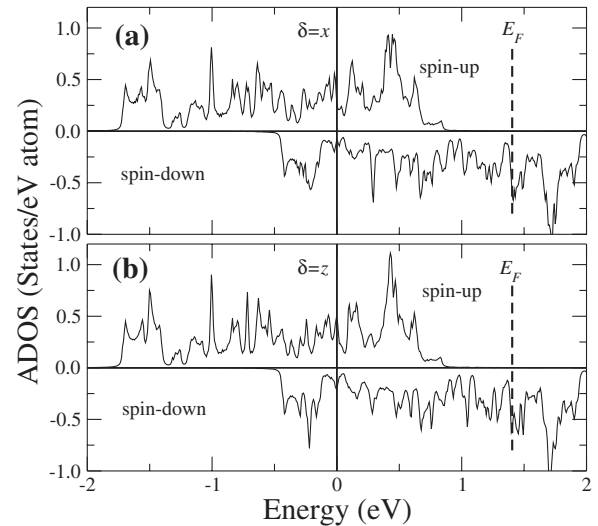


FIG. 13. Calculated ADOS for the Co_{195} nanowire shown in Fig. 7(a). In (a), we show the spin-up and spin-down bands for the direction of magnetization $\delta=x$. In (b), we show similar results but for $\delta=z$. The value of the Fermi energy (eV) is marked with a vertical dashed line.

configuration shown in Fig. 14, wherein a more abundant and less intense peaked structure is observed in the ADOS for the two orientations of the magnetization. This less degenerated spectrum (which is primarily linked to the reduced symmetry of the nanowire) leads of course to a more closely spaced energy level distribution, rendering more effective the SO mixing between occupied and empty electronic states around the Fermi level.

It is clear that the previous SO-induced modifications in the eigenvalue spectra will affect the other electronic properties in the material and, in particular, in the case of ferromagnetic atomic contacts, a strong dependence of the conductance on the direction of magnetization has already been found.²² This is physically expected since, as already stated above, when the magnetization is rotated, the energy shifts of

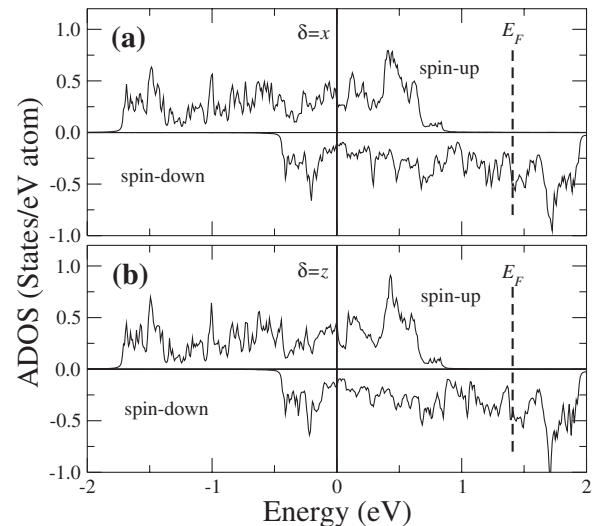


FIG. 14. Same as in Fig. 13 but for the Co_{183} nanowire shown in Fig. 7(b).

the eigenvalues as well as the band splittings obtained around the Fermi energy will play an important role in defining the number, orbital nature, and degeneracy of the conduction channels in the wires. Of course, a direct inference of the conduction from the structure of the ADOS shown in Figs. 13 and 14 is not possible but these quantities are intimately linked. In any case, it is clear that these modifications in the electronic spectra induced by precise microstructural features must be taken into account when analyzing the transport properties of more realistic magnetic nanostructures.

IV. SUMMARY AND CONCLUSIONS

In this work, we have reported extensive self-consistent electronic structure calculations dedicated to the analysis of the MAE as well as the local spin $S_{\delta}(i)$ and orbital $L_{\delta}(i)$ magnetic moments for various types of finite-length Co nanowires. We have considered monatomic chains, as well as fcc single-crystal and polycrystalline nanowires, and our calculations have revealed that the local atomic environment has a strong influence on the determination of the easy axis in the structures. We have found strong oscillations of the low energy orientation of the magnetization between the parallel and perpendicular directions as the length of the wire increases or when the geometrical details of the wire caps are modified. As a general trend, in the polycrystalline atomic configurations, we obtain reduced energy differences be-

tween the parallel and perpendicular directions of magnetization, which could imply that reducing the degree of polycrystallinity in this kind of samples could be used to synthesize magnetic nanowires with a more stable low energy magnetization direction. In addition, it is clear that due to their sensitivity to the local atomic environment, the magnetic properties of this kind of materials can be thus greatly modulated, exploring a wide spectrum of magnetic phenomena.

Finally, we have found a clear dependence of the electronic spectra on the magnetization direction. We have obtained sizable energy shifts and SO-coupling-induced removal of degeneracies all along the energy range. This effect is particularly important in the polycrystalline configurations, which implies that precise details of the microstructure (i.e., defects, grain boundaries, etc.) in magnetic nanowires are expected to also strongly modify the number of conduction channels as well as the transport properties of the wires.

ACKNOWLEDGMENTS

The authors would like to acknowledge the financial support from CONACyT (Mexico) through Grants No. 45928-F (R.A.G.-L), No. 50650 (R.A.G.-L. and J.M.M.-C), and No. 61417 (J.L.M.-L.). Computer resources from the Centro Nacional de Supercomputo (CNS) of the Instituto Potosino de Investigación Científica y Tecnológica (IPICYT), SLP, Mexico, are also acknowledged.

*guirado@ifisica.uaslp.mx

†jmmc@ifisica.uaslp.mx

‡On sabbatical leave from the División de Materiales Avanzados, Instituto Potosino de Investigación Científica y Tecnológica; moran-lopez@titan.ipicyt.edu.mx

¹T. G. Sorop, C. Untiedt, F. Luis, L. J. de Jongh, M. Kröll, and M. Rasa, *J. Appl. Phys.* **93**, 7044 (2003); J. Meier, B. Doudin, and J.-Ph. Ansermet, *ibid.* **79**, 6010 (1996); Y. H. Huang, H. Okumura, and G. C. Hadjipanayis, *ibid.* **91**, 6869 (2002); P. S. Fodor, G. M. Tsoi, and L. E. Wenger, *ibid.* **91**, 8186 (2002); X. Y. Zhang, G. H. Wen, Y. F. Chan, R. K. Zheng, X. X. Zhang, and N. Wang, *Appl. Phys. Lett.* **83**, 3341 (2003); E. Snoeck, R. E. Dunin-Borkowsky, F. Dumestre, P. Renaud, C. Amiens, B. Chaudret, and P. Zurcher, *ibid.* **82**, 88 (2003); J. B. Shi, Y. J. Chen, Y. T. Lin, C. Wu, C. J. Chen, and J. Y. Lin, *Jpn. J. Appl. Phys., Part 1* **45**, 9075 (2006).

²K. Ounadjela, R. Ferré, L. Louail, J. M. George, J. L. Maurice, L. Piraux, and S. Dubois, *J. Appl. Phys.* **81**, 5455 (1997).

³A. K. M. Bantu, J. Rivas, G. Zaragoza, M. A. López-Quintela, and M. C. Blanco, *J. Appl. Phys.* **89**, 3393 (2001).

⁴G. J. Strijkers, J. H. J. Dalderop, M. A. A. Broeksteeg, H. J. M. Swagten, and W. J. M. de Jonge, *J. Appl. Phys.* **86**, 5141 (1999).

⁵J. P. Pierce, E. W. Plummer, and J. Shen, *Appl. Phys. Lett.* **81**, 1890 (2002); L. Sun, P. C. Searson, and C. L. Chien, *Phys. Rev. B* **61**, R6463 (2000).

⁶S. Pignard, G. Goglio, A. Radulescu, L. Piraux, S. Dubois, A. Declémy, and J. L. Duvail, *J. Appl. Phys.* **87**, 824 (2000).

⁷J.-H. Gao, D.-L. Sun, Q.-F. Zhan, W. He, and Z.-H. Cheng, *Phys. Rev. B* **75**, 064421 (2007).

⁸R. Ferré, K. Ounadjela, J. M. George, L. Piraux, and S. Dubois, *Phys. Rev. B* **56**, 14066 (1997).

⁹J. M. García, A. Asenjo, J. Velázquez, D. García, and M. Vázquez, *J. Appl. Phys.* **85**, 5480 (1999).

¹⁰X. Lu, S. Ge, L. Jiang, and X. Wang, *J. Appl. Phys.* **97**, 084304 (2005).

¹¹P. S. Fodor, G. M. Tsoi, and L. E. Wenger, *J. Appl. Phys.* **93**, 7438 (2003).

¹²B. Krüger, D. Pfannkuche, M. Bolte, G. Meier, and U. Merkt, *Phys. Rev. B* **75**, 054421 (2007).

¹³B. Lazarovits, L. Szunyogh, P. Weinberger, and B. Újfalussy, *Phys. Rev. B* **68**, 024433 (2003).

¹⁴A. B. Klautau and S. Frota-Pessoa, *Phys. Rev. B* **70**, 193407 (2004).

¹⁵M. Komelj, C. Ederer, J. W. Davenport, and M. Fähnle, *Phys. Rev. B* **66**, 140407(R) (2002).

¹⁶J. Hong and R. Q. Wu, *Phys. Rev. B* **67**, 020406(R) (2003).

¹⁷J. Dorantes-Dávila and G. M. Pastor, *Phys. Rev. Lett.* **81**, 208 (1998).

¹⁸P. Gambardella, M. Blanc, K. Kuhnke, K. Kern, F. Picaud, C. Ramseyer, C. Girardet, C. Barreateau, D. Spanjaard, and M. C. Desjonqueres, *Phys. Rev. B* **64**, 045404 (2001).

¹⁹R. Druzinić and W. Hübner, *Phys. Rev. B* **55**, 347 (1997).

²⁰Y. Mokrousov, G. Bihlmayer, S. Heinze, and S. Blügel, *Phys. Rev. Lett.* **96**, 147201 (2006).

- ²¹M. C. Desjonqueres, C. Barreateau, G. Autes, and D. Spanjaard, *Phys. Rev. B* **76**, 024412 (2007).
- ²²M. Viret, M. Gabureac, F. Ott, C. Fermon, C. Barreateau, G. Autes, and R. Guirado-López, *Eur. Phys. J. B* **51**, 1 (2006).
- ²³T. Fujita, Y. Hayashi, T. Tokunaga, and K. Yamamoto, *Appl. Phys. Lett.* **88**, 243118 (2006).
- ²⁴G. M. Pastor, J. Dorantes-Dávila, S. Pick, and H. Dreyssé, *Phys. Rev. Lett.* **75**, 326 (1995).
- ²⁵J. L. Rodríguez-López, J. Dorantes-Dávila, and G. M. Pastor, *Phys. Rev. B* **57**, 1040 (1998).
- ²⁶R. Félix-Medina, J. Dorantes-Dávila, and G. M. Pastor, *Phys. Rev. B* **67**, 094430 (2003).
- ²⁷J. Friedel, P. Lengart, and G. Leman, *J. Phys. Chem. Solids* **25**, 781 (1964).
- ²⁸P. Bruno, *Magnetismus von Festkörpern und Grenzflächen* (KFA, Jülich, 1993), Chap. 24.
- ²⁹R. Haydock, in *Solid State Physics*, edited by H. Ehrenreich, F. Seitz, and D. Turnbull (Academic, New York, 1980), Vol. 35, p. 215.
- ³⁰V. Heine, *Phys. Rev.* **153**, 673 (1967).
- ³¹V. L. Moruzzi and P. M. Marcus, in *Handbook of Magnetic Materials*, edited by K. H. J. Buschow (Elsevier Science, New York, 1993), Vol. 7.
- ³²R. Guirado-López, *Phys. Rev. B* **63**, 174420 (2001).
- ³³R. A. Guirado-López and J. M. Montejano-Carrizales, *Phys. Rev. B* **75**, 184435 (2007).
- ³⁴J. Dorantes-Dávila, H. Dreyssé, and G. M. Pastor, *Phys. Rev. B* **46**, 10432 (1992); B. Piveteau, M. C. Desjonquères, A. M. Olés, and D. Spanjaard, *ibid.* **53**, 9251 (1996).
- ³⁵J. Dorantes-Dávila, H. Dreyssé, and G. M. Pastor, *Phys. Rev. B* **55**, 15033 (1997).
- ³⁶H. Wende, A. Scherz, F. Wilhelm, and K. Baberschke, *J. Phys.: Condens. Matter* **15**, S547 (2003).
- ³⁷J. B. Yang, H. Xu, S. X. You, X. D. Zhou, C. S. Wang, W. B. Yelon, and W. J. James, *J. Appl. Phys.* **99**, 08Q507 (2006).
- ³⁸A. Lessard, T. H. Moos, and W. Hübner, *Phys. Rev. B* **56**, 2594 (1997).